Experimental and theoretical evidence of the temperature-induced wurtzite to rocksalt phase transition in GaN under high pressure

Bohdan Sadovyi,[1] Małgorzata Wierzbowska,[1] Svitlana Stelmakh,[1] Silvia Boccato,[2,*] Stanislaw Gierlotka,[1] Tetsuo Irifune,[3] Sylwester Porowski,[1] and Izabella Grzegory[1]

[1]*Institute of High Pressure Physics Polish Academy of Sciences, 29/37, Sokolowska Street, 01-142 Warsaw, Poland*
[2]*ESRF-European Synchrotron Radiation Facility, Grenoble, France*
[3]*Geodynamics Research Center, Ehime University, Matsuyama 790-8577, Japan*

(Received 20 May 2020; revised 31 October 2020; accepted 5 November 2020; published 2 December 2020; corrected 3 March 2021)

The *p-T* conditions of the solid-solid phase transition from the wurtzite to rocksalt structure in GaN are determined both experimentally and by *ab initio* calculations. Experimental evaluation was based on the x-ray absorption measurements in a laser-heated diamond anvil cell. At 300 K, the transition was observed near 47 GPa. At lower pressures, the wurtzite to rocksalt transition has been induced by high temperature: 1420 K at 42 GPa and about 2100 K at 37 GPa. Thus the slope of the wurtzite-rocksalt borderline could be evaluated as negative and nonlinear. On the part of the theory, the *p-T* borderline was determined from a comparative analysis of the temperature dependences of the Gibbs potential of the wurtzite and rocksalt structures for different pressure. The Gibbs potentials were calculated within the quasiharmonic approximation and the self-consistent phonon approach. The results obtained with the self-consistent phonon approach show that the inclusion of the anharmonic phonon effects is indispensable to obtain a very good agreement with the experimental data. Possible consequences of the observed anharmonicity for the still unknown melting behavior of GaN are discussed. In particular, it is suggested that the melting temperature of the rocksalt-GaN, at pressure around 37 GPa, is not much higher than 2100 K.

DOI: 10.1103/PhysRevB.102.235109

I. INTRODUCTION

Despite the key importance of GaN based devices (Nobel Prize 2014) in optoelectronics [1] and high power electronics, some fundamental problems in GaN physics remain unsolved. This is mostly due to severe pressure requirements for thermodynamic stability of this compound at high temperatures [2,3]. The phase diagram of GaN was investigated only partially, by either experimental or theoretical methods. Basic physical properties of the Ga-N system, like GaN melting or both solid-solid and liquid-liquid phase transitions are still not determined in an undisputable way. For instance, there are principal discrepancies in the reported data on both the *p-T* conditions of GaN melting, as well as a sign of the $\mathrm{d}T^M/\mathrm{d}p$ derivative (the Clapeyron slope) [3–6]. The most relevant data on the *p-T* phase diagram of GaN are summarized in Fig. 1.

One of the unknown features of the GaN phase diagram is the boundary between the low pressure wurtzite (WZ) and high pressure rocksalt (RS) crystal phases. The only experimentally determined point of that line is at room temperature. A summary of the existing state of knowledge on the *p-T* conditions of the solid-solid phase transition in GaN including the only existing theoretical prediction [4], is presented in the area of Fig. 1 marked by the dashed line black polygon.

Experimental observations using Raman scattering, x-ray absorption spectroscopy (XAS) [7] and x-ray diffraction (XRD) [8,9] performed at room temperature (RT) in diamond anvil cell (DAC) located the solid-solid phase transition in GaN in the range of 37–52 GPa. The only existing theoretical evaluation of the solid-solid transition line was based on a semiempirical model of chemical bonding proposed by Van Vechten [4]. The Van Vechten's model predicted a transition from the wurtzite to β-tin phase near 90 GPa at room temperature which was in fundamental disagreement with the subsequent experimental data [7–9], regarding both the assumed structure of the high pressure phase and the corresponding transition pressure. In contrast, the first-principles calculations at 0 K [10–13] indicated the transition from the wurtzite to rocksalt phase, not a β-tin one. The reported results for the transition pressure were quite diverse ranging from 33 to 56 GPa, but consistent with the mentioned experimental results [7–9].

Recently, due to a significant progress in the instrumentation for the x-ray spectroscopy at extreme pressure and temperature conditions, the experimental verification of the GaN *p-T* phase diagram became feasible. In this work, we report on an experimental determination of the WZ-RS transition pressure in GaN at high temperature and on the corresponding *ab initio* calculations. The experiment was based on the XAS in a laser heated diamond anvil cell (LH-DAC), which allowed measurements at temperatures high enough to confirm implicitly the temperature induced change of the solid-solid phase transition pressure in GaN.

*Present address: Sorbonne Université, Muséum National d'Histoire Naturelle, UMR CNRS 7590, Institut de Minéralogie, de Physique des Matériaux, et de Cosmochimie (IMPMC), 75005 Paris, France.

 ©2020 American Physical Society

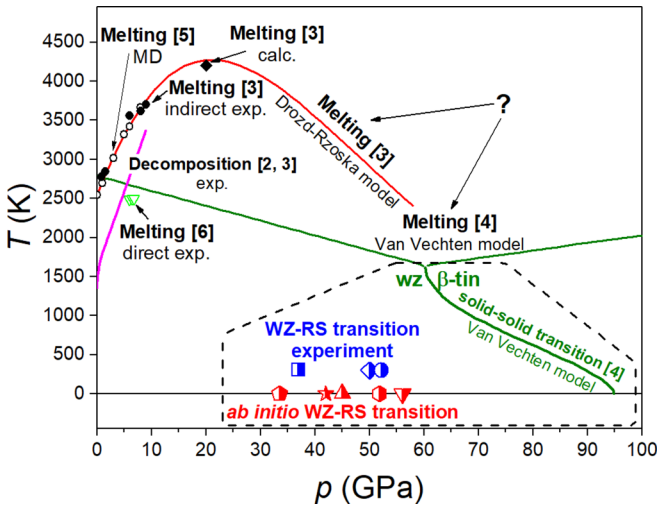

FIG. 1. State of knowledge for phase diagram of GaN. Experimental and theoretical data on GaN solid-solid phase transition (orange polygon): Van Vechten model [4] – green line; experiments at RT: EXAFS study – blue semisolid diamond [7], x-ray diffraction experiments – blue semisolid square [8] and circle [9]; *ab initio* calculations at 0 K: red semisolid pentagon [10], star and triangle [11], hexagon [12] and inverted triangle [13].

The *first-principles* approach used for evaluation of the GaN WZ-RS phase boundary was based on the comparison of the Gibbs potentials for both crystal structures. Thus, we determined a slope of the WZ-RS *p-T* curve of GaN using both: (i) the freshly obtained experimental data and (ii) the only existing for this system, the density functional theory (DFT) evaluations including anharmonic phonons via the self-consistent phonon (SCPH) approach.

II. METHODS

A. X-ray absorption spectroscopy in a laser heated diamond anvil cell

The XAS experiments at the Ga *K* edge were performed at the beamline ID24 of the European Synchrotron Radiation Facility (ESRF), Grenoble. The extended x-ray absorption fine structure (EXAFS) spectra were collected *in situ* at high pressure and temperature, in a DAC coupled with double-sided Nd:YAG LH setup [14]. To avoid the accidental appearance of strong Bragg reflections from the diamonds, a DAC with the anvils made of sintered nanopolycrystalline diamond provided by Tetsuo Irifune [15], was used.

The samples were prepared from the fine-grained powders, obtained by milling of the high structural quality and high purity GaN single crystals grown by hydride vapor phase epitaxy (HVPE) method in the IHPP PAS laboratory [16,17]. The 5 wt.% of Pt powder was admixed to the GaN powder to serve as an internal heater. GaN itself poorly absorbs the radiation of the Nd:YAG laser and the presence of the metal particles ensured the effective conversion of IR laser pulses into thermal energy. The mixture was compacted into 5-μm-thick foils and loaded into the DAC between two thin platelets of KCl that served for both thermal and chemical insulation of the sample from the anvils, as well as the pressure transmitting medium.

The pressure was applied and evaluated from the shift of the ruby fluorescence line [18] at ambient temperature prior to the heating runs. Heating experiments were conducted at fixed pressures by shooting laser pulses into a sample. The 5×7 μm^2 x-ray beam used for XAS spectra measurements was aligned with 20-μm laser spot at the sample position. The XAS spectra acquisition was synchronized to the laser pulses [14]. The temperature was determined from the spectra of radiation emitted by the hot-spot on the sample, also recorded in sync with the laser pulses from both sides of the DAC. Temperature was tuned by changing the power of the laser pulses.

The XAS measurements were performed: (i) at room temperature in the pressure range of 20–70 GPa, (ii) at fixed pressures 37 and 42 GPa in the temperature range of 300–2200 K.

B. Theoretical analysis and *ab initio* simulations of the measured EXAFS spectra

The collected EXAFS spectra were processed by publicly available software designed for the analysis of XAS, based on the IFEFFIT library of numerical and XAS algorithms [19]. These procedures allowed a determination of GaN crystal structure and its parameters at a vast range of pressure and temperature conditions. These data were used for evaluation of the experimental *p-T* borderline for the WZ-RS transition in GaN.

The raw EXAFS data were normalized with standard algorithms. The EXAFS signal $\chi(k)$ was extracted from the raw absorption data $\mu(E)$, with the ATHENA [19] program employing a smoothing spline algorithm and choosing the energy edge value (E_0) at the maximum derivative. In the normalization procedure, a line was regressed to the data in the pre-edge region from -150 to -30 eV below E_0, and a cubic polynomial was regressed in the normalization range between 30 and 370 eV above E_0. The x-ray absorption near edge structure (XANES) spectra were normalized using the ATHENA program setting the edge jump value to unity.

The measured EXAFS spectra were additionally analyzed in their XANES region by a comparison to the XANES curves simulated with the DFT computational tools: the Quantum ESPRESSO package [20] and its component, the XSPECTRA code [21]. The calculations were performed for 0 K and for pressures corresponding to the experimental conditions. The absorption cross section was calculated according to the method given in Refs. [21–23]. For the calculations, the projector-augmented-wave scheme with the plane-wave basis and the pseudopotentials for the atomic core and semicore shells were applied. The pseudopotential for the Ga atom contained a hole in the first shell. The exchange-correlation functional with the gradient correction by Perdew-Burke-Ernzerhof (PBE) [24] was used.

C. Theoretical evaluation of the WZ-RS phase boundary

For comparison with the experimental data, theoretical evaluations of the solid-solid phase transition in GaN were performed. For both rocksalt and wurtzite structures, DFT

calculations of the total energy and stress enabled to find corresponding lattice parameters and volumes (V) for the systems under pressure (Fig. S3 in the Supplemental Material [25]). The p-T borderline of the WZ-RS structural transition was determined from comparative analysis of temperature dependences of Gibbs potentials for both phases at different pressures. The point where the $G(p = const, T)$ curves for the RS and WZ structures crossed each other indicated the temperature of the phase transition at a given pressure.

The Gibbs potential might be written as a sum of the Helmholtz free energy $F(V, T)$ and the explicitly pressure-dependent term pV as follows: $G(p, T) = F(V, T) + pV$. Further, the Helmholtz free energy $F(V, T) = E_{\text{el.}}(V, T = 0) + F_{\text{vib.}}(V, T)$, is a sum of the electronic total energy term $E_{\text{el.}}(V)$ (obtained with the DFT) and vibrational contribution $F_{\text{vib.}}(V, T)$. Thus the Gibbs potential is expressed as

$$G(p, T) = \overbrace{E_{el.}(V, T = 0) + pV}^{G_I-\text{staticpart}} + F_{\text{vib.}}(V, T). \tag{1}$$

For each structure at a given pressure, the phonon frequencies, $\omega_{\mathbf{q}\nu}$, and phonon density of states (phDOS) were obtained from the density functional perturbation theory (DFPT) in the quasiharmonic approximation (QHA) [26,27]. $F_{\text{vib}}(V, T)$ was evaluated according to the QHA [28] as follows:

$$F_{\text{vib.}}^{(QHA)}(V, T) = \frac{1}{N_q}\sum_{\mathbf{q}\nu}\left[\frac{\hbar\omega_{\mathbf{q}\nu}(V)}{2} + \frac{1}{\beta}\ln\left(1 - e^{-\beta\hbar\omega_{\mathbf{q}\nu}(V)}\right)\right], \tag{2}$$

where $\beta = 1/k_{\text{B}}T$ and k_{B} is the Boltzmann constant.

However, the transition temperatures, obtained from the QHA, were strongly overestimated for lower pressures with respect to the experimental data. Therefore, in the next step, with the frozen-phonon approach, the anharmonic phonon frequencies $\Omega_{\mathbf{q}\nu}(V, T)$ and phDOS were calculated within the SCPH [29] up to the fourth order. Hence, the vibrational free energy from the SCPH was obtained according to the formula (3):

$$\begin{aligned} F_{\text{vib.}}^{(SCPH)}(V, T) &= \overbrace{F_{\text{vib.}}^{QHA}(V, T)}^{G_{II}-\text{QHApart}} + \overbrace{\Delta F_{\text{vib.}}^{\text{corr}}(V, T)}^{G_{III}-\text{SCPHpart}} \\ &= \overbrace{\frac{1}{N_q}\sum_{\mathbf{q}\nu}\left[\frac{\hbar\omega_{\mathbf{q}\nu}(V)}{2} + \frac{1}{\beta}\ln\left(1 - e^{-\beta\hbar\omega_{\mathbf{q}\nu}(V)}\right)\right]}^{G_{II}-\text{QHApart}} - \overbrace{\frac{1}{4N_q}\sum_{\mathbf{q}\nu}\left[\Omega_{\mathbf{q}\nu}^2(V, T) - \omega_{\mathbf{q}\nu}^2(V)\right]\alpha_{\mathbf{q}\nu}}^{G_{III}-\text{SCPHpart}}. \end{aligned} \tag{3}$$

Further, the Helmholtz and Gibbs free energies, and following transition temperatures, were also obtained according to the SCPH [30].

The anharmonic phonon frequencies $\Omega_{\mathbf{q}\nu}$ of the fourth order are defined as follows:

$$\Omega_{\mathbf{q}\nu}^2 = \omega_{\mathbf{q}\nu}^2 + \frac{1}{2}\sum_{\mathbf{q}_1\nu'}\Phi(\mathbf{q}\nu; -\mathbf{q}\nu; \mathbf{q}_1\nu'; -\mathbf{q}_1\nu')\alpha_{\mathbf{q}_1\nu'}, \tag{4}$$

with the harmonic phonon frequencies $\omega_{\mathbf{q}\nu}$ and the reciprocal representation of the fourth-order force constants $\Phi(\mathbf{q}\nu; -\mathbf{q}\nu; \mathbf{q}_1\nu'; -\mathbf{q}_1\nu')$. The temperature-dependent term $\alpha_{q\nu} = \hbar[1 + 2n(\Omega_{\mathbf{q}\nu})]/(2\Omega_{\mathbf{q}\nu})$ is proportional to the mean square displacement of the normal coordinate of the phonon mode $\mathbf{q}\nu$, with the Bose-Einstein distribution function $n(\beta\hbar\omega) = [\exp(\omega) - 1]^{-1}$.

The anharmonic forces were calculated up to the sixth order. Although forces higher than fourth order are not used in the SCPH equation, they were used for fitting the model to the displacement-force datasets calculated with the DFT, using the compressive sensing approach [31]. When fitting the force constants to the model, the multiple-body interactions of the negligible contributions were excluded from the anharmonic forces. The DFT forces were obtained for the displaced atomic configurations in the supercells. The displacements of 0.05 Å gave the minimal fitting error for the forces (about 3%). The 64-atom supercell for the RS structure and 32-atom supercell for the WZ structure were used. These cells were large enough to give the convergent harmonic phonons, which we checked by a comparison to the phonon spectra obtained from the DFPT. For the anharmonic phonons, a large number of displaced configurations was calculated: 410 for the WZ (34 harmonic and 366 anharmonic) and 115 for the RS structure (2 harmonic and 113 anharmonic). They originate from the next-nearest-neighbor atomic interactions included in the configurations. The interactions were considered at the distances: 3.6 Å for cubic and quartic terms for WZ and RS, 3.1 Å for fifth and sixth order terms in the WZ structure and 4.6 Å for all terms higher than harmonic in the RS structure. It has been checked that the **q**-grid densities of 8×8×8 points for the RS structure and 8×8×6 for the WZ structure lead to similar results like those obtained with the 4×4×4 **q** grid.

Technically, for the QHA [28], the DFPT implementation in the PHONON code [26,27] belonging to the Quantum ESPRESSO package [20], was used. The frozen-phonon scheme for the SCPH method [29,30], implemented in the ALAMODE code [32,33], was used for the temperature-dependent anharmonic effects. The exchange-correlation functionals within the generalized gradient approximation in the PBE flavor were applied.

III. RESULTS

A. EXAFS

As mentioned in the Sec. II, in order to confirm and refine the previously reported values [7–9], the initial measurements of the WZ-RS transition pressure by EXAFS were

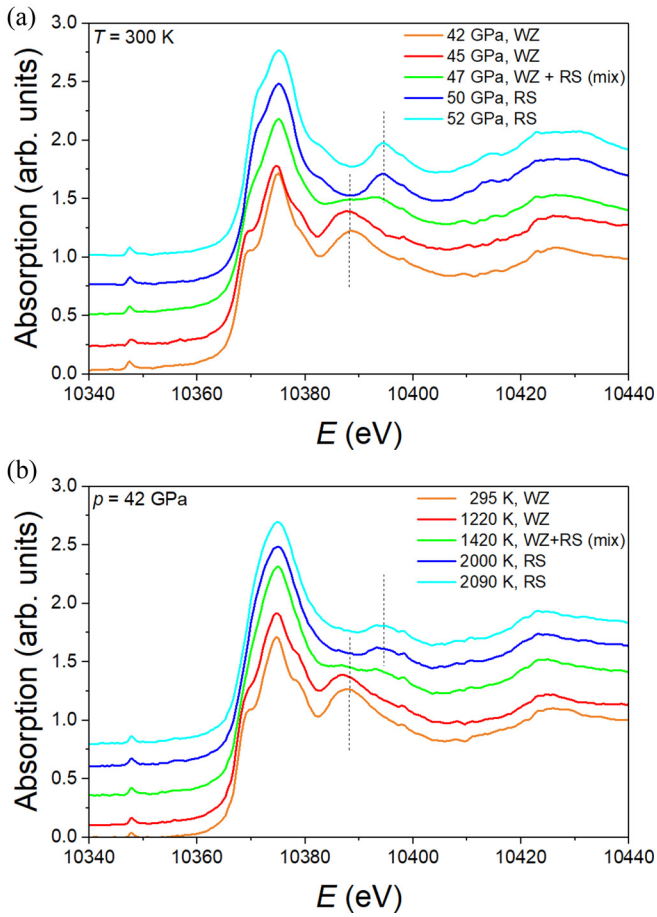

FIG. 2. (a) Normalized Ga K edge XANES obtained at RT for several pressures. (b) Normalized Ga K-edge XANES collected at a compression of 42 GPa and heated from RT to 2100 K, where the spectrum obtained at 1420 K is a fingerprint of the WZ and RS crystal mixture at the beginning of the structural transition.

performed at room temperature. The subsequent EXAFS spectra were collected at gradually increasing pressures in the range of 20–70 GPa. Up to 45 GPa, the measured spectra remained similar within the experimental error. The first meaningful change of the shape of the EXAFS curve was observed at 47 GPa. After reaching 50 GPa, the transformation of the spectrum was completed, and further increase of the pressure did not alter the shape of the curve. Several EXAFS spectra (in XANES energy range) collected in the vicinity of the phase transition are presented in Fig. 2(a).

Following the RT measurements, the high temperature experiments were performed at two chosen pressures: 42 and 37 GPa, for which the GaN wurtzite phase was stable at RT. Several XANES spectra collected at 42 GPa in the vicinity of the phase transition temperature are presented in Fig. 2(b). At 42 GPa, the pure WZ structure was stable up to 1220 K, whereas a mixture of the WZ and RS phases was observed at higher temperatures in the range of 1420–1900 K. At 1980 K and above, the pure RS phase was seen. We therefore, identified that the WZ-RS transition at 42 GPa started between 1220 and 1420 K.

At 37 GPa the EXAFS spectrum corresponding to the pure RS phase appeared at 2100 ± 100 K. However the exact position where this transition started was not determined. We could just conclude that it should take place below 2100 ± 100 K.

Thermal pressure at the applied experimental conditions calculated for GaN in isochoric case is about 2.4 GPa. The actual pressure increase in the DAC due to increased temperature is expected to be of the order of 50% of the isochoric value [34] which in our case means 1–1.5 GPa. This figure is of the order of accuracy of the pressure measurement with the ruby method. In the following discussion, we will use pressure values from the room temperature measurements, keeping in mind that they may be slightly underestimated with respect to actual figures.

For the room temperature experiments, the spectra collected between 45 and 50 GPa could be naturally explained as a mixture of those of the low- and high- pressure phases. Figure 3(a) demonstrates the application of the linear combination analysis [35] that allows us to plot the fitting line for 47 GPa spectrum as a weighted superposition of 55% of the WZ and of 45% of the RS experimental curves. Thus, we have concluded that the transition was direct, without any (meta-) stable intermediate structures involved. The same has been observed for the transition induced by temperature [Fig. 3(b)].

The structures of both low- and high-pressure phases were confirmed by comparison of the experimental curves to the simulated spectra and by numerical analysis of the experimental data. The experimental curves obtained below and at 45 GPa matched the simulated XANES spectra of the WZ structure whereas those obtained at 50 GPa and above, matched the simulations of the RS structure. The XANES of the low-and high-pressure phases differed around the first local minimum and the second maximum in the measured spectra. The same features appeared in the simulated XANES of the WZ and RS structures as it shown in Fig. 4.

In the range of 30–60 GPa, the variation of the features of the simulated XANES curves with pressure was very weak for both WZ and RS phases as it is shown in the [25], in Figs. S2a and S2b. In contrast, their dependence on the polarization of the electric field, especially for the WZ phase, was relatively strong (Fig. S2c in [25]).

Processing of the experimental data by derivatives of the DEMETER software package [19], ATHENA and ARTEMIS also confirmed the WZ and RS structures appearance (Fig. S2 in Ref. [25]) and yielded the relative atomic volume change at the phase transition of about 14.5% as shown in Fig. S3 [25]. Pressure dependences of the atomic volume for the WZ and RS phases were also obtained from DFT calculations and these data are in a very good agreement with experiments (Fig. S3 in Ref. [25]).

The combined experimental and theoretical approaches used in this study enabled us to confirm both the pressure and temperature-induced structural WZ to RS phase transition in GaN.

The transition pressure derived from the EXAFS measured at RT is in good agreement with the previous report on the phase transition in GaN at 300 K [7] evaluated by a similar method and this transition pressure is in the 45–47 GPa range.

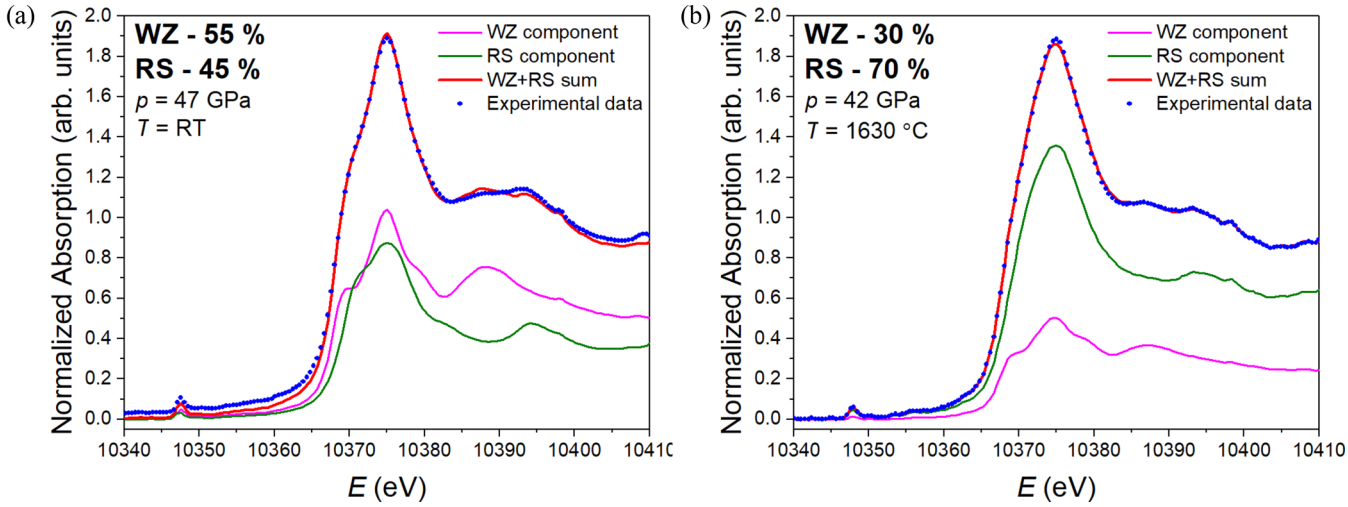

FIG. 3. (a) Normalized XANES spectrum from 47 GPa, RT compared with fitted curve that was obtained as a simple algebraic sum of 55% of the WZ (standard – normalized XANES from 39 GPa) and of 45% of the RS (standard – normalized XANES from 55 GPa) experimental curves. (b) Normalized XANES spectrum from 42 GPa, 1630 K compared with fitted curve which was obtained as a simple algebraic sum of 30% of the WZ (standard – normalized XANES from 42 GPa, 1000 K) and of 70% of the RS (standard – normalized XANES from 42 GPa, 2000 K) experimental curves.

B. Gibbs potentials for wurtzite and rocksalt GaN

The phonon spectra for the WZ and RS structures obtained with the DFPT scheme (harmonic phonons) and the SCPH (anharmonicity included up to the fourth order) do not contain the soft-phonon modes for all pressures in the range of 0–45 GPa. If phonons were calculated for the rocksalt structure in a small supercell containing eight atoms (instead of a two-atom elementary cell), then at the pressures lower than 45 GPa some soft-phonon modes would appear, indicating the phase transition to the WZ structure (the elementary cell with four atoms). The pressure dependence of the phDOS at zero temperature is presented in Figs. S4a and S4b in Ref. [25]. The temperature dependence of the phDOS at the pressure of 43 GPa is presented in Figs. S4c and S4d in Ref. [25]. An effect of the anharmonicity in the WZ and RS structures has the opposite sign of the phonon frequency shift.

The pressure and temperature dependence of the free energy components: static part [$E^{\mathrm{DFT}} + pV$, G_I in Eq. (1)], harmonic part [$F_{\mathrm{vib.}}^{QHA}$, G_{II} in Eq. (3)] and anharmonic part [SCPH correction, G_{III} in Eq. (3)] is presented in Fig. 5.

For each structure, WZ and RS, the total Gibbs energy was calculated for the pressures in the range from 34 to 46 GPa.

As it is shown in Fig. 5(b), the effect of temperature is much stronger than the effect of pressure in this energy scale. In Fig. 5(c), the fingerprint of the anharmonic frequency shift is reflected in the opposite effect of the SCPH part of Gibbs free energy of the WZ and RS. The effect of anharmonicity is stronger in the WZ than the RS structure.

C. Wurtzite-rocksalt phase boundary

Points of the intersection of the theoretically calculated Gibbs free energy curves (as functions of T at a given p) for

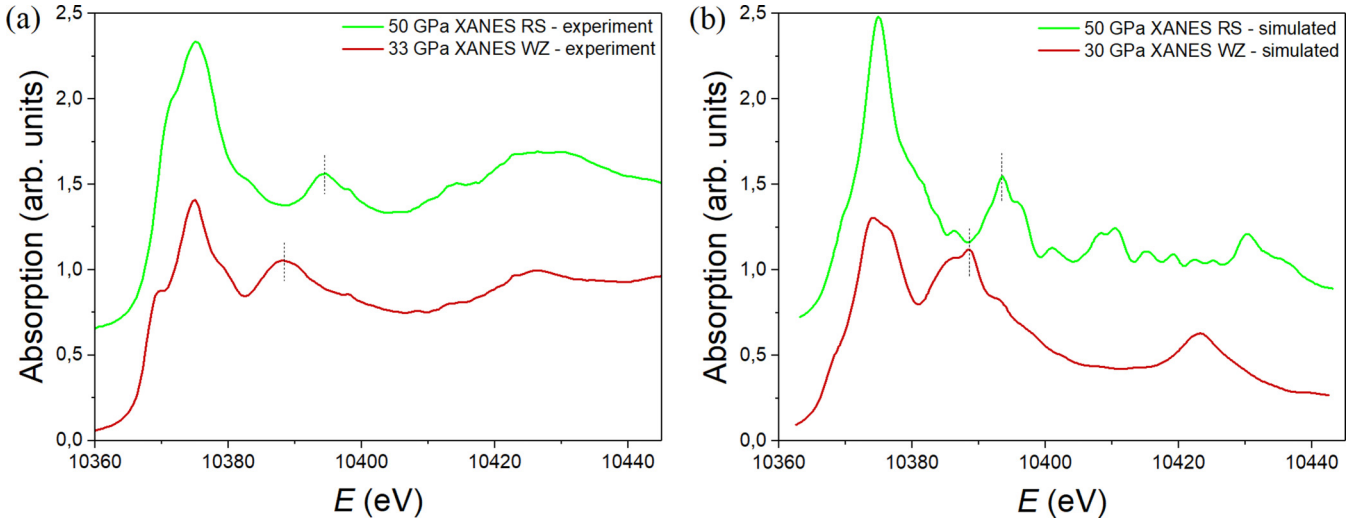

FIG. 4. (a) Experimental XANES spectra of WZ and RS phases, (b) Simulated XANES spectra of the WZ and RS phases.

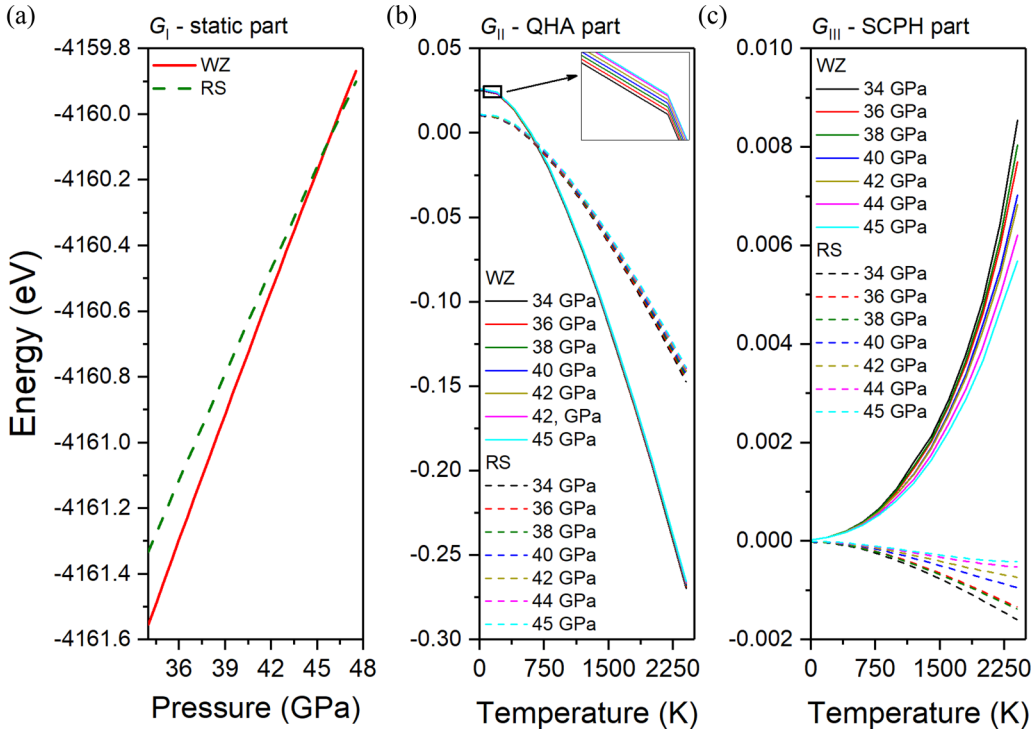

FIG. 5. A comparison of the components of Gibbs free energies obtained for the WZ and RS structures: (a) static part from Eq. (1), (b) harmonic part – QHA from Eq. (2), and (c) SCPH correction from Eq. (3).

the WZ and RS structures indicated the equilibrium between the two solid phases of GaN as it is shown in Fig. 6; blue points guided by a blue line.

Analysis of the pressure and temperature evolution of the measured XANES, reported in Figs. 2(a) and 2(b), lead to the experimental points on the *p-T* phase diagram for the WZ-RS phase transition presented in Fig. 6 (red points guided by a red line). It is evident from our measurements that the boundary between the low-pressure WZ and the high-pressure RS phases on the *p-T* phase diagram of GaN has a negative slope, i.e., the transition pressure decreases at higher temperatures.

The theoretical *p-T* equilibrium line for the WZ and-RS phases, which includes the anharmonic phonon effects (blue plot in Fig. 6), is in a good agreement with the experimental data. In particular, the negative slope of the temperature dependence is well reproduced.

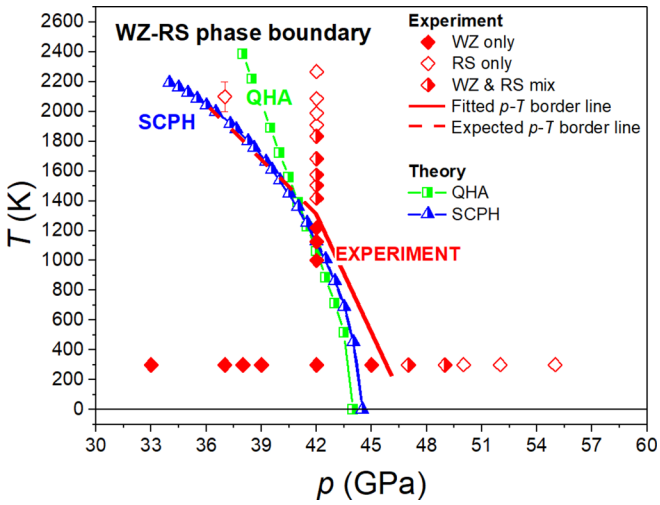

FIG. 6. Comparison of the phase boundary for the WZ to RS transition obtained experimentally as well as calculated with the DFT Gibbs potentials with only harmonic phonons (QHA) and including the anharmonic phonon effects (SCPH).

IV. DISCUSSION

As it was already mentioned, the room temperature WZ-RS transition pressure of 47 GPa evaluated in this work, is in a very good agreement with values coming from earlier reports: 47 GPa (EXAFS, Ref. [7]) and 52.2 GPa (XRD, Ref. [9]). On the other hand, it is apparently higher than the one reported in [8] (37 GPa, XRD). This discrepancy was discussed in Ref. [9] where it was suggested that a different way of monitoring the pressure in DAC, applied in Ref. [8] could lead to the observed disagreement. In Refs. [7,9] as well as in the present study, the pressure was measured with the ruby fluorescence method, while in Ref. [8] the equation of state of gold was used for pressure calibration. Also the value of bulk modulus of GaN following from the measurement reported in Ref. [8] (188 GPa) was much lower than the commonly accepted value of 210 GPa [36]. These inconsistencies suggest that the value of 37 GPa reported in Ref. [8] for the WZ-RS transition pressure in GaN was too low.

The LH DAC experiment at 42 GPa where the WZ-RS transition has been induced by heating (transition started at 1420 K) clearly indicated that high temperature stabilizes the rocksalt phase of GaN. The observation of the temperature

induced WZ-RS transition at 37 GPa at 2100 ± 100 K, additionally supports the existence of the high temperature RS phase. This transition was observed at much lower temperature than could be derived from a linear extrapolation of the experimental line drawn through (47 GPa, 300 K) and (42 GPa, 1420 K) experimental points. On the other hand, the WZ-RS phase boundary evaluated theoretically with the harmonic phonons only (QHA) was linear at nonzero temperature, and consistent with the low temperature experimental data mentioned above. The slope of the QHA line towards lower pressures, at temperatures higher than 1500 K, was much smaller than that of the curve, which includes the anharmonic effects; see Fig. 6. Therefore, both experimental and theoretical results of this study indicated a significant influence of the anharmonicity on physical properties of the GaN crystal lattice, starting at temperatures as low as ~1500 K.

A similar effect has been reported for AlN [37], where it was also shown theoretically, that the WZ-RS phase boundary is strongly nonlinear due to the phonon anharmonicity. It was even suggested that the extension of the rocksalt stability range could reach zero pressure, which would prevent melting of AlN from its wurtzite phase. Moreover, the visible influence of the anharmonicity on the WZ-RS phase boundary shape in AlN appeared, as for GaN, at temperature as low as 1500 K, which was believed to be about ½ of the AlN melting point.

As it is shown in Figs. S4c and S4d in Ref. [25], the effect of phonon anharmonicity in the WZ and RS structure in GaN is opposite with respect to the phonon frequency shift. Consequently, the Gibbs potential for the WZ phase increases with inclusion of the anharmonic terms, whereas it decreases for the RS structure. This is different from the earlier reported results for AlN where anharmonicity in both RS and WZ phases shifts the phonon frequencies in the same way.

Interestingly, for GaN, according to the results of this study, the impact of anharmonicity is stronger in the WZ than the RS structure. This is again opposite to the case of AlN, reported in Ref. [37], where the RS structure was much more sensitive to the anharmonicity than the WZ one.

These observations indicate that the mechanisms of the WZ to RS phase transition in GaN and AlN are different. Such a suggestion is consistent with earlier reports where stability of the wurzite GaN, InN and AlN has been considered. In particular, it was shown [9] that in GaN, both the lattice constants a and c decreased with pressure at a same rate thus the axial ratio c/a remained virtually constant. It was in strong contrast to the lattice behavior of both InN and AlN where the axial ratio apparently decreased under the pressure and the resulting deformation lead to a collapse of the wurzite lattice into the rocksalt one. The different properties of GaN crystal lattice with respect to both InN and AlN are reflected in its much higher WZ to RS transition pressure of 47 GPa (this study) compared to 12 GPa [9] and 23 GPa [9] for InN and AlN, respectively.

The result of this work is an excellent starting point for evaluation and understanding of the full phase-diagram of GaN including determination of the GaN melting curve, which is still an open question [3,38]. As follows from our data, for pressures higher than 37 GPa, the melting of GaN

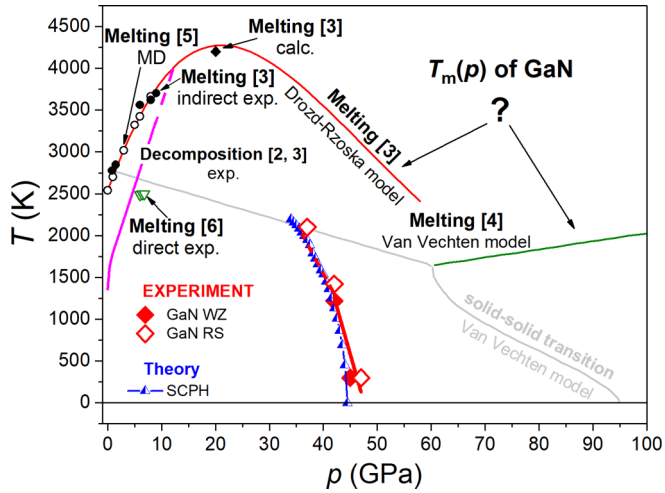

FIG. 7. Updated vision of the p-T phase diagram of gallium nitride: the solid-solid WZ-RS borderline (red, experimental, blue, theoretical) is a contribution of this study.

is expected to occur in the rocksalt phase due to the temperature induced WZ-RS phase transition in 37–47 GPa pressure range. In particular, at 37 GPa the melting temperature should be higher than 2100 K, where we have observed the crystalline rocksalt GaN. The melting curve of the RS GaN should intersect the WZ-RS boundary at the triple-point, where the wurtzite, rocksalt, and liquid phases meet together.

An updated vision of the p-T phase diagram of GaN including our data, as well as the most relevant references, is shown in Fig. 7.

It is worth noting that observation of melting of GaN in its WZ phase seems to be a challenge because the pressure window for the existence of this phase at high temperature, is limited from both low and high pressure sides. For low pressures, the limiting factor is thermal decomposition of the WZ GaN (purple line in Fig. 7) whereas for high pressures, it is a temperature induced WZ-RS phase transition (blue line).

The experimental technique used in this study seems to be a good choice to complete the challenging diagram of Fig. 7. However, due to extreme temperatures expected for melting, some technical improvements for heating of GaN would be helpful. Two options are considered for near future experiments: a more sophisticated way of distributing of the internal heat absorber in the GaN powder, e.g., by Pt sputtering or by going to the CO_2 laser, which can heat the wide bandgap crystals directly [39], without utilizing intermediate radiation absorbers.

For theory, it seems that a simulation of GaN melting in its both rocksalt and wurtzite structures would be crucial to guide future experiments. Approaching the WZ-RS-liquid triple point from the high pressure side is especially suitable since thermal decomposition of the crystal in the RS phase is no longer an obstacle for melting. Strong anharmonic behavior of GaN at temperatures used for experiments in this study, clearly suggests that the melting temperature of the RS-GaN, at pressure around 37 GPa, is not much higher than 2100 K. A molecular dynamics modeling, which is in progress, should confirm this suggestion very soon.

V. SUMMARY

The *p-T* conditions of the solid-solid phase transition from the wurtzite to rocksalt structure in GaN were determined both experimentally and by *ab initio* calculations. The experimental evaluation was based on the x-ray absorption measurements in a laser-heated diamond anvil cell. At 300 K, the transition was observed near 47 GPa. At lower pressures, the WZ to RS transition has been induced by high temperature: 1420 K at 42 GPa and about 2100 K at 37 GPa. Thus the slope of the WZ-RS borderline could be evaluated as negative and nonlinear.

The theoretical XANES spectra were determined for the WZ and RS phases at various pressures to confirm the structures corresponding to the observed spectra.

Further, the Gibbs potentials were calculated for both structures according to the QHA and SCPH schemes and the phase diagram was obtained. The effect of phonon anharmonicity in the WZ and RS structure in GaN is opposite with respect to the phonon frequency shift. The WZ Gibbs potential increases with inclusion of the anharmonic terms and it decreases for the RS structure. This is different than the earlier reported anharmonic effects in AlN where both effects of the anharmonicity in RS and WZ shift the phonon frequencies in the same way.

The possible consequences of the observed anharmonicity for the still unknown melting behavior of GaN were discussed. In particular, it is suggested that the melting temperature of the rocksalt-GaN, at pressure around 37 GPa, is not much higher than 2100 K.

ACKNOWLEDGMENTS

We are extremely grateful to Dr. S. Pascarelli and Dr. R. Torchio for the excellent scientific hosting of our team at ESRF ID24. Valuable scientific discussions and the technical support of Dr. A. Rosa from ESRF are greatly appreciated. The access to ESRF was financed by the Polish Ministry of Science and High Education, Decision No. DIR/WK/2016/19. The calculations have been performed in the Academic Computer Center "Cyfronet" Cracow, Poland, using the PROMETHEUS computing cluster. The experimental part of this study was supported by the Polish Grant No. OPUS 12 No UMO-2016/23/B/ST5/02728 of the National Science Center.

[1] The Nobel Prize in Physics 2014 (Nobel Media AB), www.nobelprize.org/nobel_prizes/physics/laureates/2014/.
[2] J. Karpinski, J. Jun, and S. Porowski, J. Cryst. Growth **66**, 1 (1984).
[3] S. Porowski, B. Sadovyi, S. Gierlotka, S. J. Rzoska, I. Grzegory, I. Petrusha, V. Turkevich, and D. Stratiichuk, J. Phys. Chem. Solids **85**, 138 (2015).
[4] J. A. Van Vechten, Phys. Rev. B **7**, 1479 (1973).
[5] K. Harafuji, T. Tsuchiya, and K. Kawamura, J. Appl. Phys. **96**, 2501 (2004).
[6] W. Utsumi, H. Saitoh, H. Kaneko, T. Watanuki, K. Aoki, and O. Shimomura, Nat. Mater. **2**, 735 (2003).
[7] P. Perlin, C. Jauberthie-Carillon, J. P. Itie, A. San Miguel, I. Grzegory, and A. Polian, Phys. Rev. B **45**, 83 (1992).
[8] H. Xia, Q. Xia, and A. L. Ruoff, Phys. Rev. B **47**, 12925 (1993).
[9] M. Ueno, M. Yoshida, A. Onodera, O. Shimomura, and K. Takemura, Phys. Rev. B **49**, 14 (1994).
[10] A. M. Saitta and F. Decremps, Phys. Rev. B **70**, 035214 (2004).
[11] F. S. Saoud, J. C. Plenet, L. Louail, and D. Maouche, Comput. Theor. Chem. **964**, 65 (2011).
[12] N. E. Christensen and I. Gorczyca, Phys. Rev. B **50**, 4397 (1994).
[13] A. Munoz and K. Kunc, Comput. Mater. Sci. **2**, 400 (1994).
[14] M. Mezouar, R. Giampaoli, G. Garbarino, I. Kantor, A. Dewaele, G. Weck, S. Boccato, V. Svitlyk, A. D. Rosa, R. Torchio, O. Mathon, O. Hignette, and S. Bauchau, High Press. Res. **37**, 170 (2017).
[15] T. Irifune, A. Kurio, S. Sakamoto, T. Inoue, and H. Sumiya, Nature (London) **421**, 599 (2003).
[16] T. Sochacki, M. Amilusik, B. Lucznik, M. Bockowski, J. L. Weyher, G. Nowak, B. Sadovyi, G. Kamler, I. Grzegory, R. Kucharski, M. Zajac, R. Doradzinski, and R. Dwilinski, Proc. SPIE **8625**, 86250B (2013).
[17] T. Sochacki, M. Amilusik, B. Lucznik, M. Fijalkowski, J. L. Weyher, B. Sadovyi, G. Kamler, G. Nowak, E. Litwin-Staszewska, A. Khachapuridze, I. Grzegory, R. Kucharski, M. Zajac, R. Doradzinski, and M. Bockowski, Jpn. J. Appl. Phys. **53**, 05FA04 (2014).
[18] L. Liu, Y. Bi, and J.-A. Xu, Chin. Phys. B **22**, 056201 (2013).
[19] B. Ravel and M. Newville, J. Synchrotron Radiat. **12**, 537 (2005).
[20] P. Giannozzi, S. Baroni, N. Bonini, M. Calandra, R. Car, C. Cavazzoni, D. Ceresoli, G. L. Chiarotti, M. Cococcioni, I. Dabo, A. Dal Corso, S. de Gironcoli, S. Fabris, G. Fratesi, R. Gebauer, U. Gerstmann, C. Gougoussis, A. Kokalj, M. Lazzeri, L. Martin-Samos, N. Marzari, F. Mauri, R. Mazzarello, S. Paolini, A. Pasquarello, L. Paulatto, C. Sbraccia, S. Scandolo, G. Sclauzero, A. P. Seitsonen, A. Smogunov, P. Umari, and R. M. Wentzcovitch, J. Phys.: Condens. Matter **21**, 395502 (2009).
[21] M. Taillefumier, D. Cabaret, A.-M. Flank, and F. Mauri, Phys. Rev. B **66**, 195107 (2002).
[22] C. Gougoussis, M. Calandra, A. P. Seitsonen, and F. Mauri, Phys. Rev. B **80**, 075102 (2009).
[23] O. Bunau and M. Calandra, Phys. Rev. B **87**, 205105 (2013).
[24] J. P. Perdew, K. Burke, and M. Ernzerhof, Phys. Rev. Lett. **77**, 3865 (1996); **78**, 1396(E) (1997).
[25] See Supplemental Material at http://link.aps.org/supplemental/10.1103/PhysRevB.102.235109 for details of theoretical calculations and figures that are not included in the main text.
[26] S. Baroni, P. Giannozzi, and A. Testa, Phys. Rev. Lett. **58**, 1861 (1987).
[27] S. Baroni, S. de Gironcoli, A. Dal Corso, and P. Giannozzi, Rev. Mod. Phys. **73**, 515 (2001).
[28] S. Baroni, P. Giannozzi, and E. Isaev, Rev. Mineral. Geochem. **71**, 39 (2010).
[29] N. R. Werthame, Phys. Rev. B **1**, 572 (1970).
[30] T. Tadano and S. Tsuneyuki, Phys. Rev. B **92**, 054301 (2015).

[31] F. Zhou, W. Nielson, Y. Xia, and V. Ozolins, Phys. Rev. Lett. **113**, 185501 (2014).

[32] T. Tadano, Y. Gohda, and S. Tsuneyuki, J. Phys.: Condens. Matter **26**, 225402 (2014).

[33] Y. Oba, T. Tadano, R. Akashi, and S. Tsuneyuki, Phys. Rev. Mater. **3**, 033601 (2019).

[34] D. Andrault, G. Fiquet, J.-P. Itié, P. Richet, P. Gillet, D. Häusermann, and M. Hanfland, Eur. J. Mineral. **10**, 931 (1998).

[35] M. Benfatto and C. Meneghini, in *Synchrotron Radiation*, edited by S. Mobilio, F. Boscherini, and C. Meneghini (Springer, Berlin, 2015).

[36] A. Polian, M. Grimsditch, and I. Grzegory, J. Appl. Phys. **79**, 3343 (1996).

[37] N. Shulumba, Z. Raza, O. Hellman, E. Janzen, I. A. Abrikosov, and M. Oden, Phys. Rev. B **94**, 104305 (2016).

[38] S. Porowski, B. Sadovyi, I. Karbovnyk, S. Gierlotka, S. J. Rzoska, I. Petrusha, D. Stratiichuk, V. Turkevich, and I. Grzegory, J. Cryst. Growth **505**, 5 (2019).

[39] B. Shukla, N. V. Chandra Shekar, N. R. Sanjay Kumar, T. R. Ravindran, P. Sahoo, S. Dhara, and P. C. Sahu, J. Phys.: Conf. Ser. **377**, 012014 (2012).

Correction: The name and affiliation of the sixth author were missing in the original publication and have been inserted. Reference [15] contained incorrect source information and has been fixed. The grant number in the last sentence of the Acknowledgments contained an error and has been set right.